International Journal of Heat and Mass Transfer 52 (2009) 260–270

Contents lists available at ScienceDirect

International Journal of Heat and Mass Transfer

journal homepage: www.elsevier.com/locate/ijhmt

Convective heat transfer in liquid microchannels with hydrophobic and hydrophilic surfaces

Shou-Shing Hsieh *, Chih-Yi Lin

Department of Mechanical and Electro Mechanical Engineering, National Sun Yat-Sen University, Kaohsiung 80424, Taiwan, ROC

ARTICLE INFO

Article history:
Received 6 November 2007
Received in revised form 23 May 2008
Available online 16 July 2008

ABSTRACT

Experiments were performed to study the heat transfer characteristics of channel flows of deionized (DI) water, methanol, 50 wt% DI water/50 wt% methanol mixture, and ethanol solution in asymmetrically (one sided heating) heated rectangular microchannels with an aspect ratio (H/W) of 0.56 and the corresponding hydraulic diameters (D) of 129 μm at $5 \leqslant Re \leqslant 240$. Local heat transfer coefficients distribution were recorded with both isothermal (273 K) and isoflux (12.6, 18.1, 32.3, 50.5 mW/mm^2) heating. The influences of test liquid mass flow rates, test fluids, heating condition (isothermal vs isoflux), and surface condition (hydrophilic vs hydrophobic) on heat transfer behavior were examined. Thermal entrance length were also found and correlated in terms of the relevant parameters.

1. Introduction

Research in microfluidics has become particularly active for a few years, and the literature is now full of novelty dealing with particular applications of fundamental aspects [1–3]. One of the earliest pioneering work in the area of microchannels was provided by Tuckerman and Peace [4] at Stanford University in the early 1980s. From then on, a number of technical articles have been published in this area of microchannels as they related to applications, automotive, chemical, and aerospace industries.

Microchannel heat sinks are of special interest as high efficiency cooling devices due to several advantages such as small cooling demand and dimensions, which directly result in enhanced convective heat transfer. Consequently, much work has gone into the development of microchannel technology recently. Up to now, with regard to flows through microchannels, the knowledge is more advanced for gaseous than for liquid flows [5]. However, in some cases like advanced heat sink designs as applied to microprocesser cooling with average chip heat fluxes in the range of 40–60 W/cm^2, air cooling may not be appropriate. On the contrary, single phase liquid flow through the microchannels would be expected and acceptable. In addition, the relatively few works available in the literature in the area of microscale thermal-hydraulics reveal that there are still relevant disagreement among the results [5,6]. In particular, most disagreements pertain to laminar flow and laminar-to-turbulent flow transition and the corresponding friction factors as well [7,8]. Heat transfer tests reveal that microchannels have a better performance than the conventional flow channels [9]. However, Qu et al. [10] have studied heat transfer of water flow in trapezoidal silicon microchannels and found that the Nusselt number (Nu) is much lower than the conventional theory.

Furthermore, Celata et al. [11] have found the Nu is Reynolds number dependent in both laminar and turbulent regime for R-114 flowing through a stainless steel tube with a diameter of 130 μm. Herwig and Hausner [12] proposed a new concept to explain why experiments in micro-flow devices always show differences compared to the corresponding situations in micro-system. They pointed out the micro effects can be considered as scaling effects for conventional large systems. The proposed concepts can also explain the unusual Nu distribution in a laminar microchannel flow reported in Tso and Mahulikar [13]. Since the bulk temperature of the flow was not measured inside the microchannel, their judgment and conclusion are still in question. A review article written by Morini [14] has reported that either Nusselt number increases/or decreases with Reynolds number increase was found in the laminar regime. In addition, the Reynolds analogy fails in microchannels. Based on these results, it is concluded that there is still a considerable scatter in the existing heat transfer data [6]. In spite of this, some related correlation for thermally developing and fully developed condition about liquid microchannel heat transfer data can still be listed in Table 1.

More recently, Hetsroni et al. [22] have reported that there seems no significant discrepancy in Nu value with different cross section (circular, triangular, rectangular, and trapezoidal) microchannels as compared to those of conventional channels, and they concluded that the deviations are due to experimental errors. Mishan et al. [23] have firstly used infrared camera to visualize the detailed temperature distribution in a water rectangular microchannel of $D_h = 440$ μm and, again, they found that there is no noted difference from the conventional channels based on the

* Corresponding author. Tel: +886 7 5252000x4215; fax:+886 7 5254215.
E-mail address: sshsieh@faculty.nsysu.edu.tw (S.-S. Hsieh).

0017-9310/$ - see front matter © 2008 Elsevier Ltd. All rights reserved.
doi:10.1016/j.ijheatmasstransfer.2008.05.021

Nomenclature

C_p	specific heat, J/μgK	P	pressure, bar
D	channel hydraulic diameter, μm	Pr	Prandtl number
H	heat transfer coefficient defined in Eq. (6), W/m^{2}K	Q	Volumetric flow rate, mm^3/s
h_m	mean heat transfer coefficient defined in Eq. (10), W/m^{2}K	q''	heat flux, mW/mm^2
		Re	Reynolds number
$\bar{h}$	average heat transfer coefficient defined in Eq. (8), W/m^{2}K	T_i	fluid inlet temperature, K
		T_o	fluid outlet temperature, K
k	thermal conductivity, W/mK	T_w	local wall temperature, K
I	electric current, amp	u	average liquid velocity, mm/s
I_m	μLIF image intensity, gray	u_{max}	the maximum flow velocity, mm/s
L	channel length, μm	V	voltage, V
ℓ	length scale of the channel, μm	x	downstream distance, μm
Nu	local Nusselt number defined in Eq. (4)	μ	dynamic viscosity, Pas
$\overline{Nu}$	average Nusselt number defined in Eqs. 8 and 11, and also the fully developed Nusselt number	ρ	density, μg/m^3
		ΔT_m	log mean temperature difference defined in Eq. (9), K
$\dot{m}$	mass flow rate, μg/s		

Table 1
Some related laminar thermally fully developed and developing correlation of $\overline{Nu} = cRe^m\ Pr^n$ and $Nu = c(Gz^{-1})^m$

Reference	Parameters	Correlation	Condition and restrictions
W. Qu et al. [10]	D = 168.9 μm L = 30 mm	Laminar and thermally fully developed flow $\overline{Nu} = 1 \sim 2$ ($100 < Re < 400$), $\overline{Nu} = 2$ ($400 < Re < 1500$)	Silicon trapezoidal microchannel (hydrophobic)
Incropera and DeWitt [15]		$\overline{Nu} = 4.36$ (constant heat flux) $\overline{Nu} = 3.66$ (constant wall temperature)	Laminar and thermally fully developed (tube channel)
X.F. Peng et al. [16]	D = 133–367 μm L = 50 mm	Laminar and thermally fully developed flow $\overline{Nu} = C_{H,l} Re^{0.62}\ Pr^{0.33}$, $50 < Re < 4000$	$C_{H,l}$ depended on aspect ratio $0.01 < C_{H,l} < 0.058$
X.F. Peng et al. [17]	D = 133–343 μm L = 50 mm	Laminar and thermally fully developed flow $\overline{Nu} = 0.117\ (D/W_c)^{0.81}\ (H/W)^{-0.79} Re^{0.62}\ Pr^{0.33}$, $50 < Re < 4000$	W_c: center-to-center distance of microchannels
Wu and Cheng [18]	D = 110 μm L = 34 mm	Laminar and thermally fully developed flow $\overline{Nu} = 0.5 \sim 2.6$ (hydrophilic), $50 < Re < 600$ $\overline{Nu} = 0.5 \sim 2.3$ (hydrophobic), $50 < Re < 600$	Silicon trapezoidal microchannel with (hydrophilic)/ without (hydrophobic) SiO_2
L. Zhuo et al. [19]	D = 102 μm L = 30.5 mm	Laminar and thermally fully developed flow $\overline{Nu} = 0.8 \sim 2.35$, $25 < Re < 450$	Silicon trapezoidal microchannel (hydrophobic)
P. X. Jiang et al. [20]	W = 200 μm H = 600 μm D = 300 μm L = 20 mm	Laminar and thermally developing flow Without micro-porous: $Nu = 0.52\ (Gz^{-1})^{-0.62}$, $Gz^{-1} \leqslant 0.05$ $Nu = 2.02\ (Gz^{-1})^{-0.31}$, $Gz^{-1} > 0.05$ (thermally fully developed) With micro-porous: $Nu = 1.97\ (Gz^{-1})^{-0.72}$, $Gz^{-1} < 0.05$	Rectangular microchannel with/without micro-porous (one-sided heating)
S. Shen et al. [21]	W = 300 μm H = 800 μm L = 50 mm	Laminar and thermally developing flow $Nu = 0.505\ (Gz^{-1})^{-0.22}$, $0.0375 < Gz^{-1} < 0.14$ $Nu = 2.18$, $Gz^{-1} > 0.14$ (thermally fully developed)	Rectangular microchannel (one-sided heating)
Present study	W = 180 μm H = 100 μm D = 129 μm L = 20 mm $Pe = 20 \sim 3300$	Laminar and thermally fully developed flow Hydrophilic microchannel:constant heat flux: $\overline{Nu} = 2.62$ Constant wall temperature: $\overline{Nu} = 2.49$ Hydrophobic microchannel: constant heat flux: $\overline{Nu} = 2.42$ Laminar and thermally developing flow $Nu = 0.968\ (Gz^{-1})^{-0.36}$, $Gz^{-1} \leqslant 0.063$ $Nu = 2.62$, $Gz^{-1} > 0.063$ (thermally fully developed)	A rectangular microchannel array(hydrophilic and hydrophobic) Aspect ratio: 0.56

pressure drop, heat transfer, and thermal entry length measurements.

Based on the foregoing discussion, it is necessary to further study the basic heat transfer phenomena and document the important information in different working fluids of DI water, methanol, 50 wt % DI water/50 wt% methanol mixture, and ethanol solution microchannel flow of two different surface properties of hydrophilic and hydrophobic microchannels with isothermal (@273 K) and isoflux (@12.6, 18.1, 32.3, 50.5 mW/mm^2) via different measuring techniques such as μPIV and μLIF. Detailed operating condition and related parameters are listed in Table 2. Furthermore, the conventional thermal entrance length Le_{th} was also examined and discussed, which has seldom been reported before. In this study, the objective was focused on the convective heat transfer of the four different fluids flowing through a 100 μm × 180 μm (H × W) asymmetrically heated microchannel with uniform heat flux and constant wall temperature, respectively. The main features of the study will include the thermal entrance length, downstream wall and bulk temperature distribution as well as local Nu distribution. Moreover, comparisons will be made with previous results of the similar studies and those of conventional large channels to further

Table 2
Experimental parameters and uncertainties of relevant parameters

Working fluids	DI water	Methanol (99%)	Water (50%) + Methanol (50%)	Ethanol (99%)
Experimental parameters				
Rhodamine B concentration (M)	1.86×10^{-5}	1.2×10^{-5}	1.53×10^{-5}	10^{-5}
Tracing particle Concentration (mL^{-1})	2×10^8 particles mL^{-1}			
Temperature calibration (°C)	$T = -0.084I_m + 98.6$ (I_m: μLIF image)			
Constant Heat flux q'' (mW/mm^2)	12.6, 18.1, 32.3, 50.5			
Constant Wall temperature T_W (K)	273			
Flow and temperature measured position	x = 0, 5, 10, 15, 20 mm			
Flow rate (sccm)	0.6 ~ 56.3			
Reynolds number, *Re*	5 ~ 240			
Peclet number, *Pe*	20 ~ 3300			
Parameters of strip heater and power supply				
Constant voltage (V)	5, 6, 8, 10			
Constant current (A)	0.23, 0.27, 0.36, 0.45			
Ohm (Ω)	22			
r (effective coefficient accounting for heat loss)	0.84			
Total energy (W)	0.95, 1.37, 2.44, 3.82			

Geometric and parameters	System error (%)	Random error (%)
Uncertainties of geometric dimensions and relevant parameters		
L (μm)	±0.015	±0.08
H (μm)	±0.33	±0.92
W (μm)	±1.67	±0.46
D (μm)	±2.63	±1.72
u (mm/s)	±0.02	±3.12
μLIF image intensity (I_m)	±1.38	±3.62
Calibration(μLIF)	±2.36	±3.31
T (°C) from μLIF	±3.16	±4.17
T (°C) from Thermocouple	±0.43	±2.86
Power (W)	±0.063	±0.36
Re	±2.63	±3.56
h	±3.59	±4.08
Nu	±4.47	±4.45

examine the size effect for different working fluids and surface property.

2. PDMS microchannel fabrication

The PDMS microchannels were fabricated in house at the University Microsystem laboratory by casting twenty straight open channels (i.e., channel array) from PDMS methyl acrylate (Dow Corning Co.) and sealed with the same material with specific gravity of 1.08, viscosity of 3900 mPas, and thermal conductivity 0.18 W/mK at the temperature of 25 °C, respectively. The casting mold was made by SU-8 deep UV lithography. Detailed SU-8 mold design and PDMS channel fabrication through deep UV lithography can be explained as follows. The fabrication starts with silicon wafers insulated by thermal oxidation. The SU-8 photoresist is spin-coated at 2000 rpm onto silicon wafers to create masters for 30 s with 100 μm in thickness. A mask is made out of high-solution quartz glass printed to scale to put on the silicon wafers, and then a UV beam (365 nm) is illuminated for a few minutes to make a negative etched channel manifold. During the process, the excess photoresist is peeled off from the silicon substrate that has a negative pattern of the master. Meanwhile, a 10 (PDMS):1 (curing agent) mixture of PDMS prepolymer was poured onto the master and cured for 1 h at 70 °C. After curing the PDMS replica mold was peeled from the master. Flat pieces of PDMS were formed by casting prepolymer against a silicon wafer and curing. To form enclosed channels, a PDMS replica and a 0.18 mm thickness cover glass (Superior Marienfeld, refraction index n = 1.518) were used and bonded by hot pressing to enclose the microchannel. Then, it was rinsed in acetone as well as in ethanol and dried with argon stream. The present surface property can be switched from hydrophobicity to hydrophilicity by using one of energetic surface treatments like UV radiation (UV/ozone) and plasma exposure for 30 minutes.

For these twenty channels, precise information of the channel's dimension is extremely important for an accurate evaluation on convective heat transfer in microchannels. The depth, width, and length were measured optically with an uncertainty of less than ±0.2%. To understand the present device surface condition, the roughness of the channel was measured along its center with the surface profilometer. The uncertainties for relevant geometric parameters are also listed in Table 2. The resultant channels were examined by an electron microscope. These twenty microchannels have the same respective dimensions and characteristics.

In order to observe hydrophobic and hydrophilic surface effect on fluid and heat transfer mechanism, both surface condition were tested and associated data were measured. Further, to investigate both flow and heat transfer characteristics of a liquid flowing through microchannels, heating condition for the present microchannel/test section was shown in Fig. 1, for constant heat flux and constant wall temperature, respectively.

3. Experimental

3.1. Test facility and loop

Deionized (DI) water with another three fluids were used as the working fluid. The test liquid was circulated in a closed loop, as shown in Fig. 1, which had provision for filtering, metering, heating and cooling. The maximum operating pressure of the loop is 40 kPa, while the maximum specific flow rate 57 sccm. The test system allows simultaneous power control, wall temperature measurement, as well as optical imaging of the flow visualization.

The microchannel flow loop is mounted to a fixture with relevant flow components. The main part was a strip of 200 μm wide and 200 μm thick strip type microheater made of aluminum with a heated section of 10 mm × 20 mm (nominal) exposed to the test fluid. The heat input has implemented on either side (top for isoflux and bottom for isothermal) of the active section which was connected (via AWG 20 lead wire), in turn, to power leads. The test section was thermally insulated by fiberglass to minimize heat losses.

Temperature measurements were performed via fifty-two T type thermocouple wires located on respective positions as also shown in Fig. 1. These fifty-two thermocouples had been divided into two groups. One group (only two thermocouples are needed) is for channel upstream plenum and downstream plenum temperature reading; the other group of the remainder fifty thermocouples was broken into five sets for the wall temperature measurements at five respective downstream locations. Namely, each set/or location has ten thermocouples which gives the temperature reading for the chosen channels (10 channels were chosen) at a given location. Noting that both micro strip-heaters and thermocouples were flush mounted to, and insulated from, the channel walls. There is only one-side heating either isothermal/or isoflux on the channel bottom or top floor. This thermal boundary condition gives an asymmetrically heating; however, the surface temperature of top and bottom floor were measured to examine laterally heat conduction (conjugate effects). As stated previously, the bulk fluid temperature was measured in the fluid just upstream and downstream of the microchannel using two 80 μm T type

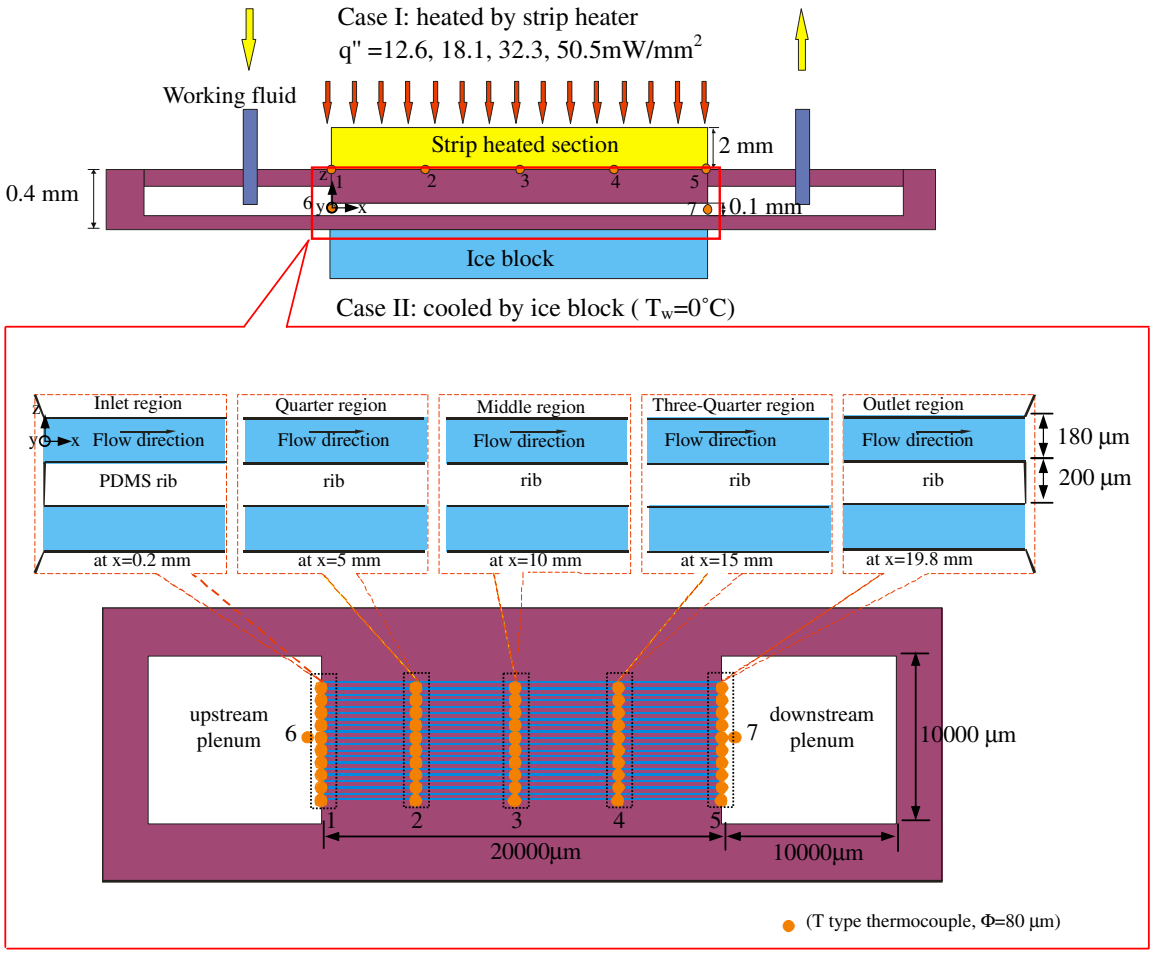

Fig. 1. Schematic of the test microchannel.

thermocouples. Based on an energy balance, the heat losses can be doubly examined. Two pressure transducers, placed at the inlet and outlet of the section, respectively, were use to measure the pressure drop over the entire channel. The inlet temperature measured for the test fluids is about 23 °C.

The voltage drop across the heater was measured directly. The current was determined from the voltage drop across a calibrated resistance shunt mounted in series with the circuit. The heat generation was determined as a product of the measured voltage and current. The power input was adjusted with Q = 0.95 to 3.82 W. As stated earlier, the average temperature of DI water was also measured at the inlet and exit of the test channel. Temperature readings from thermocouples sensors located at the top and bottom of the insulation layer underneath the microheaters showed the power losses by conduction to be typically 5% of the heat input. Radiation losses were estimated to be less than 1% of the generated power. The conduction and radiation losses were incorporated into data reduction analysis and subtracted from the heat generation in each run. Thermodynamics properties of DI water, such as density, viscosity, thermal conductivity were found from a conventional water table. Data for thermally developing entry length and fully developed heat transfer coefficient are presented and discussed.

3.2. Flow (μPIV)/temperature (μLIF) visualization

A schematic drawing of the experimental setup to implement MPIV/micro laser-induced fluorescence (μLIF) measurement is shown in Fig. 2. The study combines μPIV and μLIF to measure velocities and temperature simultaneously. The use of the μPIV technique is very attractive in microfluidics because it helps to understand the detailed flow phenomena in microsystems. The μPIV utilizes flow tracing particles to map the flow in the microchannels. In the study, red polystyrene fluorescent latex particles (Duke Scientific Corp.) with 0.93 μm diameter were used as seeding. These particles had an excitation peak of 532 nm (green) and an emission peak at 612 nm (red). These particles were surfactant-free. These particles were introduced into the microchannel and pressure driven by a range of pressure drop. Fluorescence imaging of the rhodamine B (Sigma–Aldrich Co.) dye was performed for temperature μLIF measurement. The values of the present microchannel dimensions and geometric sizes as well as the relevant parameters and associated properties were tabulated in Table 2.

The system whose layout is reported in Fig. 2 is based on two pulsed Nd: YAG lasers (New Wave Solo II, 30 mJ/pulse, double cavity) firing on the second harmonic (green 532 nm). The laser provides a thin sheet with measured thickness. The light sheet is positioned to illuminate the entire inlet, outlet, and mid-section of the channel. The laser pulse duration is 4-80 ms based on the velocity magnitude. The test system is mounted on a movable xz stage on an inverted epifluorecent microscope (DMILM Leica) with 10 ×, numerical aperture NA = 0.25 panchromatic objective and a field view of 800 × 600 μm^2. The measurement plane (i.e., object plane) was precisely positioned relative to the test section by moving the objective lens vertically in the *y* direction and by moving the table horizontally in the *x* and *z* directions. The concentration

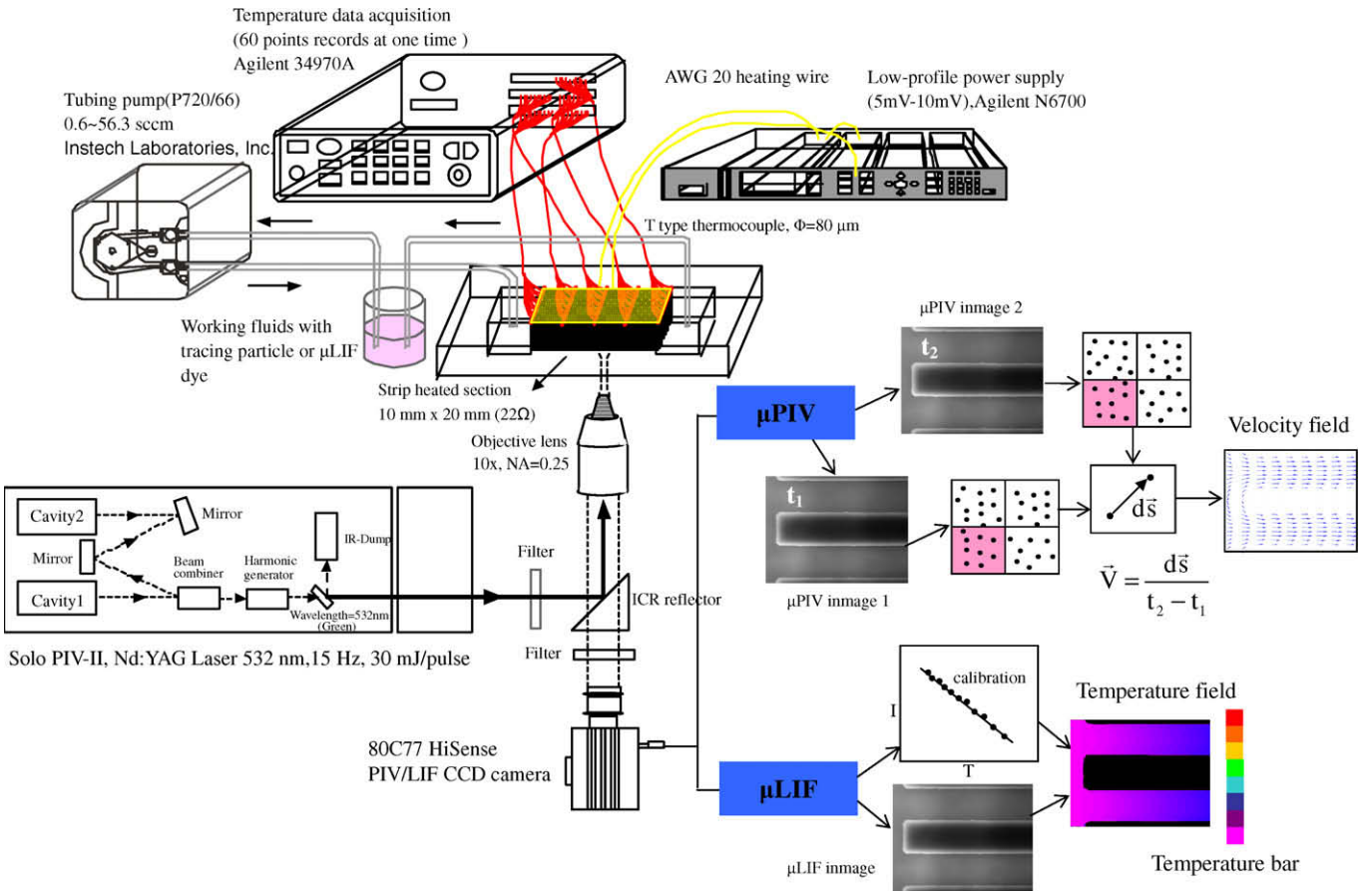

Fig. 2. Schematic of test channel and μPIV/μLIF system.

of fluorescent microspheres based on interrogation volume was 2×10^8 particles per milliliter.

The images were recorded using a Dantec 80C77 Hisense PIV $1344 \times 1024 \times 12$ bit interline transfer camera. A total of five images per second were taken for each flow field with a spatial resolution of 32×32 pixels, and the interrogation cell overlap was 50%. Ensemble averaging of 20 images consecutively captured for 4 s was used to obtain the velocity measurements. The calculated measurement depth of the present μPIV is 27 μm. The present measurements were performed in a clean room of the University Microsystem Laboratory where the ambient temperature was controlled at 298.2 K. Each measurement was repeated at least three times at a specified condition. The present measurements were conducted at the first quarter, the middle region, the three quarter, and at inlet as well as exit regions of the microchannel, and the flow was found to be reached thermally fully developed before the exit region of the microchannel.

3.3. Temperature visualization experiments

The visualization of the local fluid temperature was achieved with the same apparatus as used for flow visualization and measurements; namely, Fig. 2. Instead of using a fluorescent particle, however, the channel was filled with a solution of rhodamine B, which is a fluorescent dye showing a temperature-sensitive quantum yield in the range of 0–100 °C. Calibration was done by means of a simple conduction problem in the pure water that can be solved analytically. With this, the temperature scale can be read through the related equation listed in Table 2. Uncertainty due to μLIF measurement was found to be less than ±0.09 °C. Experiments were conducted with a fluorescence microscope equipped with a long-working distance 10× objective. The images were recorded using the same equipments with those used for μPIV measurements. From the captured images, the detailed temperature distribution can be extracted. The intensity values of the captured images then were converted to temperature using the intensity vs temperature calibration.

4. Data reduction and uncertainty

The experiments were carried out under steady state conditions. For each different set of experimental runs, the data including flow rates, liquid temperatures, inlet and outlet pressures, the test section top/bottom wall temperatures, and the input voltage and current were continuously measured and recorded using a digital acquisition system based on an IBM PC. The parameters used in the data reduction and analysis are summarized below:

Hydraulic diameter

$$D = \frac{4A}{P} = \frac{2WH}{(W+H)} \tag{2}$$

Reynolds number

$$Re = \frac{\rho u D}{\mu} \tag{3}$$

where u stands for the average channel velocity and the local Nusselt number, *Nu* was defined as

$$Nu = \frac{hD}{k} \tag{4}$$

Properties of the working fluid were evaluated at the film temperatures, 0.5 ($T_w + T_i$). The experimental data were finally reduced in terms of local heat transfer coefficient, and the associated Nusselt number with different Reynolds numbers.

As stated previously, the heat flux of the microchannel structure was defined as

$$q'' = \frac{Q}{A} \tag{5}$$

where Q is a net heat input (=VI-heat losses) and A is the surface area of the channel. Therefore, the heat transfer coefficient can be calculated by

$$h(x) = \frac{q''}{T_w(x) - T(x)} \tag{6}$$

where $T_w(x)$ is secured through exterior surface temperature measurements with 1-D heat conduction correction for interior surface temperature (i.e. $T_w(x)$), and the local bulk mean temperature of $T(x)$ is obtained by an energy balance giving

$$T(x) = T_i + \left(\frac{Q}{\dot{m}C_p L}\right)x \tag{7}$$

Therefore, the local bulk mean temperature from the experiments can be doubly checked by using energy balance as flow proceeds downstream. It was found the maximum deviation less than 3.2% for the worst case. There are two heat transfer coefficients; a local as stated previously and an averaged were determined. The local heat transfer coefficient was found in Eq. (6) and the corresponding average Nusselt number is defined as

$$\overline{Nu} = \frac{\bar{h}D}{k} \tag{8}$$

and $\bar{h}$ is defined as $\bar{h} = \frac{\sum_i^n h_i \Delta x_i}{L}$. Eqs. (6)–(8) were used to calculate the relevant heat transfer parameters for constant heat flux. While, for constant wall temperature, the "mean heat transfer coefficient (h_m)" and its corresponding Nusselt number can be applied using the log mean temperature difference

$$\Delta T_m = \frac{(T_{w,i} - T_i) - (T_{w,o} - T_o)}{\ln\left(\frac{T_{w,i} - T_i}{T_{w,o} - T_o}\right)} \tag{9}$$

$$\text{and } h_m = \frac{\dot{m}C_p(T_o - T_i)}{A\Delta T_m} \tag{10}$$

$$\overline{Nu} = \frac{h_m D}{k} \tag{11}$$

where $T_{w,i}$ and $T_{w,o}$ denote the wall temperature at the fluid entering and exiting the channel. Finally, the above-calculated local Nu are presented as a function of the downstream distance and Reynolds number, and the average $\overline{Nu}$ was plotted against the Pe number.

The uncertainty in measured local heat transfer coefficients was estimated to be less than ±5%. The largest contribution to the uncertainty comes from the temperature measurements (±0.5 °C). Uncertainty in Reynolds numbers was found to be within ±3%.

5. Results and discussion

Before a set of formal tests, μLIF temperature measurements should be tested and calibrated properly and accurately. One of typical calibrated distribution was performed at $Pe = 40$ for deionized water (not shown). It is seen that the color evolution in temperature was in good agreement in the sense of temperature development with those of conventional large tubes, which indicates an adequate initial condition as well as boundary condition that the present test apparatuses had. In addition, the corresponding flow/velocity field is also secured. The maximum axial conduction number (M) and viscous heating factor (κ) reported in Celata et al. [24] were found to be small ($M \leqslant 0.018$ and $\kappa \leqslant 4.46\%$) for the present cases under study, which give both the axial conduction effect and the viscous heating can be considered negligible.

5.1. Flow/velocity field

Velocity calibration was performed and compared with those of analytical solutions within deviation less than ±4%. The present μPIV velocity vector plot (one out of ten microchannels was shown) in fully developed flow regime was obtained by averaging velocity data over twenty consecutive images for the case of $Pe = 39.6$ of the DI water along the downstream distance on the hydrophilic and hydrophobic surface of the channel, respectively. Enlarged views are shown that, at $x = 10.2$ mm, there is slip on hydrophobic wall. Basically, these two velocity profiles seem no significant difference in the core region of the channel, where the flow exhibits a laminar parabolic-like profile except near the wall. The slip effect can clearly be noted (not shown). In fact, one may find the local velocity at wall is about 4 mm/s at $Pe = 39.6$.

5.2. Slip velocity vs hydrophobic surface

Although the best wall velocity measurement can be only reached at $z = (\mp 90 \pm 9.3/2)$ μm, the slip velocity at wall can still be obtained by extraplation of the present measured velocity profile. Taking a closeup examination of the present hydrophobic and hydrophilic property of the working fluid interaction with the channel surface, it is found that, after the channel surface being treated by UV/ozone for a thirty minutes, the resultant channels with different working fluids such as water, methanol, water (50%) + methanol (50%) and ethanol have been proven to be hydrophilic. Fig. 3(a) shows one of the results for water. In fact, in addition, even with no surface treatment, methanol channels, in Fig. 3(b), are still hydrophilic with a contact angle less than 90°, which had been measured after the images of wetting characteristic were taken from a high resolution camera. One of typical local wall velocity vector does show a zero velocity near the wall. On the other hand, for the untreated channels with water and water (50%) + methanol (50%), the results shown in Fig. 3(c) exhibit hydrophobic characteristic whose contact angle is bigger than 90° with a nonzero velocity near the wall for water. Such slip ratio (defined as u_s/u) also illustrated in Fig. 3(c), respectively was found to be 10% for water, which is in good agreement with those reported from Tretheway and Meinhart [25] and about 4% for water and methanol mixture (not shown). Here u_s is the slip velocity at wall and u is the average velocity at that particular downstream location. Furthermore, based on the pressure drop measurements for different test fluids, the friction factor (f) can be extracted and found to be $f = 61.5/Re$ for non-slip condition and $f = 59.7/Re$ for slip condition; while, the conventional channel is $f = 61.2/Re$ with the same aspect ratio of 0.56. This f is almost the same as the former for non-slip condition and a little bit bigger than the latter as one would expect.

5.3. μLIF/temperature visualization

Generally, a detailed temperature distribution at the channel entrance region (⩽100 μm) for all the test fluids can be drawn through μLIF measurements (only for isoflux cases). Fig. 4 shows a particular case of the working fluid of water at a particular location of $x = 0$ (inlet), 0.5(1/4 region), 1(middle), 1.5 (3/4 region) and 2 (outlet) mm along downstream for entire channel of the corresponding Pe of 39.6 at a volumetric flow rate (Q) of 17.5 mm^3/s with a mild temperature range of 23–50 °C. The color evolution following the order of appearance, from decent red, blue, light blue,

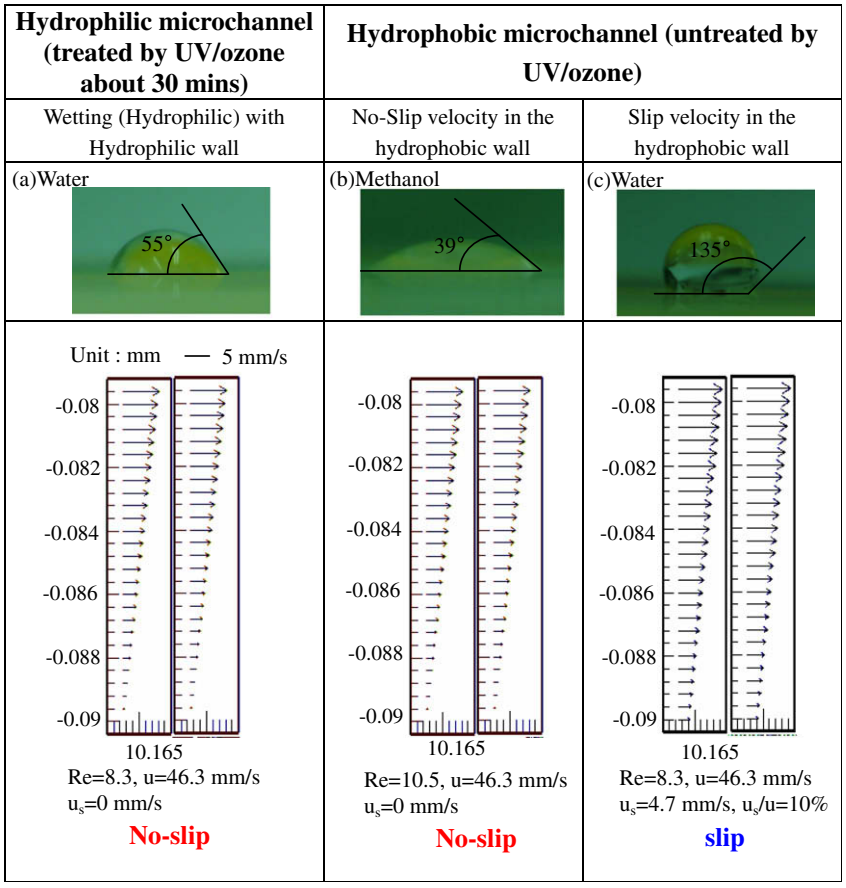

Fig. 3. Flow vector with/without slip velocity at the wall of hydrophilic and hydrophobic microchannel.

and, finally, green shown in temperature distribution along downstream clearly indicated that the convective seems significant as compared to the diffusion. This situation becomes stronger as *Pe* increases with a quick color change (not shown). Both the temperature variation ($\Delta T \approx 27$ °C) and the variation through color transition can clearly be noted. Among all the cases studied herein, the

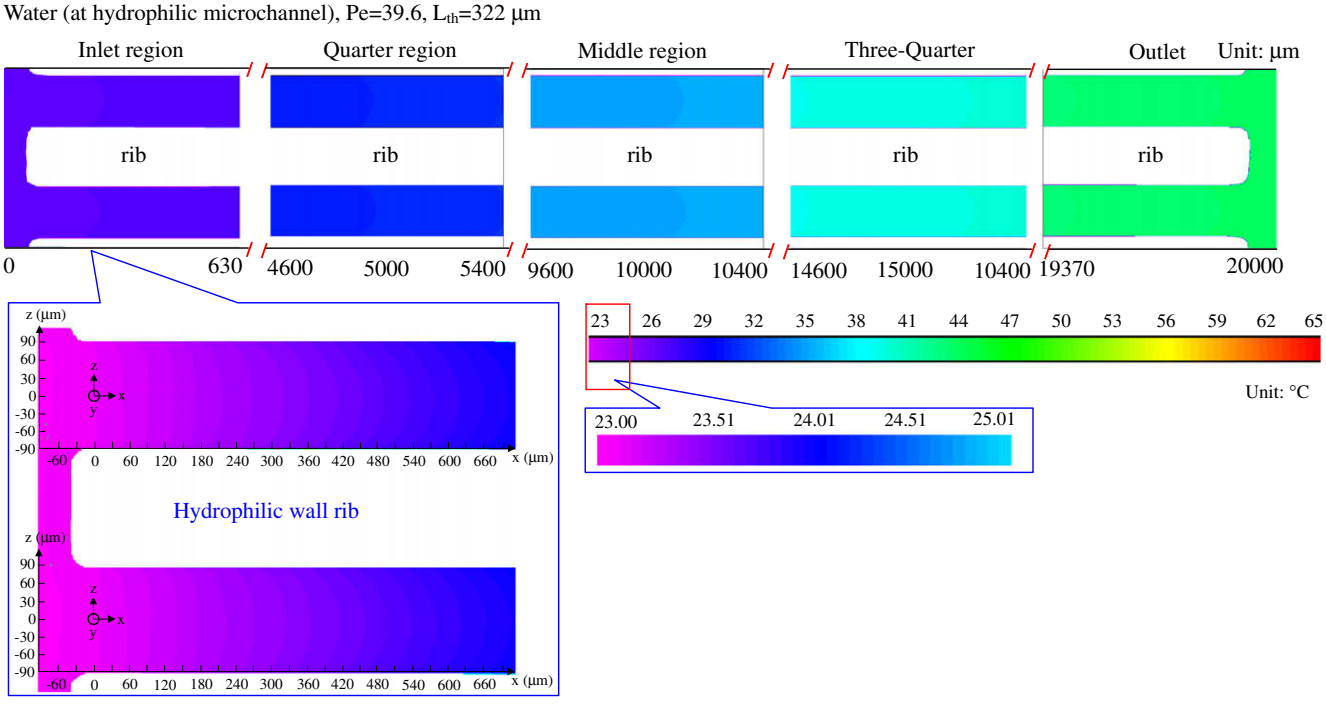

Fig. 4. Temperature distribution at $x = 0$, 0.5, 1, 1.5, 2 mm of water in hydrophilic microchannel at $Q = 17.5$ mm^3/s.

maximum temperature difference between channel inlet and outlet is found to be about 45 °C. At this stage, the color transition covers a larger spectrum as compared to that of Fig. 4 following the order of appearance, from purple, blue, light blue, green, yellow, and, finally, to orange.

5.4. Local heat transfer coefficient distribution and thermal entry length

After the temperature distribution along the downstream distance extracted from μLIF visualization, the local wall temperature as well as the channel fluid bulk mean temperature can thus be calculated, and so is the local Nusselt number (Nu). The local Nusselt number (Nu) can be plotted as a function of $x/(DPe)$, an inverse of the Graetz number (Gz), as presented in Fig. 5, for all the cases under study. The distribution can also be correlated in the form of

$$Nu = 0.968(\mathrm{Gz}^{-1})^{-0.36} 0 < \mathrm{Gz}^{-1} \leqslant 0.063$$

with the experimental data within ±5%. The power dependence (0.36) on Gz^{-1} is very similar to that of the traditional cases (≈1/3) as $0 \leqslant \mathrm{Gz}^{-1} \leqslant 0.01$. The value of this exponent seems to be in between those of Jiang et al. [20] and Shen et al. [21]. This value is perhaps quite sensitive to the physical geometry of the channel and thermal boundary conditions.

Following Fig. 5, the thermal entry length can be obtained. In fact, the value can be read out in Fig. 5 as the Nu distribution is independent of downstream distance, and it is found to be 0.063 which is a little bit higher than those of the conventional tubes (0.05), which indicates that the present microchannels have a longer thermal entrance length. The power low correlation can be developed in Fig. 6 as $\mathrm{Le}_{\mathrm{th}}$ was plotted against Pe for different surface condition. Further examination of the thermal entry length, it is found that the hydrophobic channel has a longer length than that of hydrophilic as expected. This can be seen from the coefficient of the power law correlation (0.069 vs 0.063). Both results are in good agreement with that [26] where the thermal entry length was reported to be $\mathrm{Le}_{\mathrm{th}} \approx 0.0625\ Pe_{\mathrm{th}}$ for an infinite parallel plate. In addition, in a microsystem, the Nusselt number ($=h\ell/k$) can be found in the form of a function of Pe_{th} only via dimensional analysis. Also included in Fig. 6 are the hydrodynamic entry length for hydrophobic and hydrophilic channels, respectively. Again, the former seems to have a little bit longer length (0.064 vs 0.061).

5.5. $\overline{Nu}$ vs Pe and compared with those of previous studies

Fig. 7 presents the fully developed Nusselt number as a function of Pe number only as stated previously. For both constant heat flux ($q'' = 18.1\ \mathrm{mW/mm^2}$) and constant temperature ($T_0 = 273$ K) with four different working fluids, a flat profile (i.e. $\overline{Nu} \approx$ const) was noted for DI water for both hydrophilic and hydrophobic microchannels with a much higher $\overline{Nu}$ of hydrophilic walls. This situation prevails for another working fluids like mixture of water and methanol, methanol, and ethanol. Generally, $\overline{Nu}$ of isoflux is bigger than that of isothermal case. For both heating condition, DI water has the highest $\overline{Nu}$ followed by the mixture of water and methanol, methanol and ethanol. In fact, the $\overline{Nu}$ of methanol and ethanol seems the same. Further, the present results were compared with those of previous studies [18,19] with the same working fluid (DI water). The agreement seems good as $Pe \geqslant 2000$. Unlike Wu and Cheng [18] and Zhuo et al. [19], the present results do show a nearly constant $\overline{Nu}$ as $Pe \leqslant 2000$. The reasons for this difference are perhaps due to the existence of the axial conduction in those reported results from [22]. Similar behavior happens in Fig. 8 for $\overline{Nu}$ vs Pe distribution with different heat flux.

The $\overline{Nu}$ values of all the test fluids studied herein for one-sided heating as shown in Fig. 8 was found to be nearly a constant (≈2.63) for the entire Pe under study. This value seems little bit lower than the conventional rectangular channels with the same aspect ratio [27]. This is perhaps partly because they two have the different thermal boundary condition on the bottom floor (our case is diabatic) and partly because the present local bulk mean temperature was obtained over z direction and not from the conventional y direction. In spite of this, it is still a little bit higher than those of the traditional fully developed $\overline{Nu}$ for the same aspect ratio rectangular channel (4.03) with one sided heating. But, it seems in good agreement with those of Shen et al. [21] for rectangular micro channels with one-sided heating listed in Table 1 where a value of 2.18 was found, and it is a constant regardless of what the test fluid is. Moreover, the effect of heat flux variations on $\overline{Nu}$ was also examined as shown in Fig. 8 for DI water. Surface properties effect is again clearly noted in Fig. 8 from

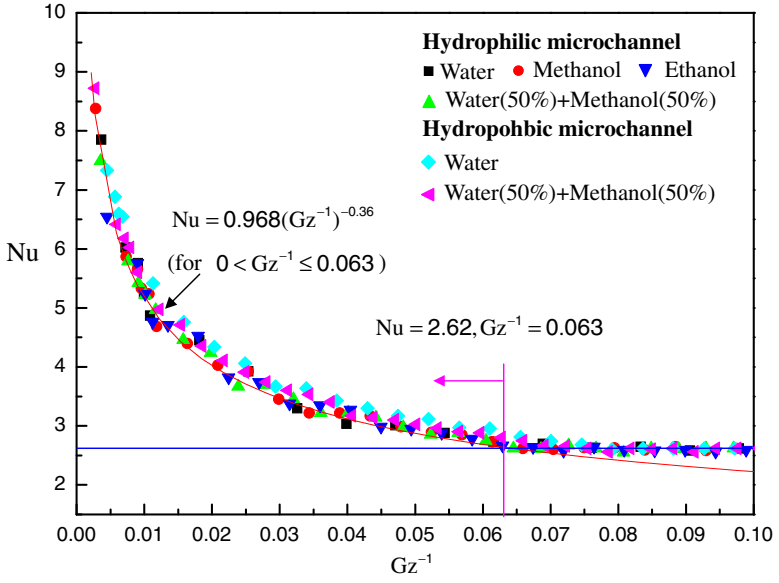

Fig. 5. The correlation of the entrance length for hydrophilic and hydrophobic microchannel at constant heat flux q″ = 18.1 mW/mm^2.

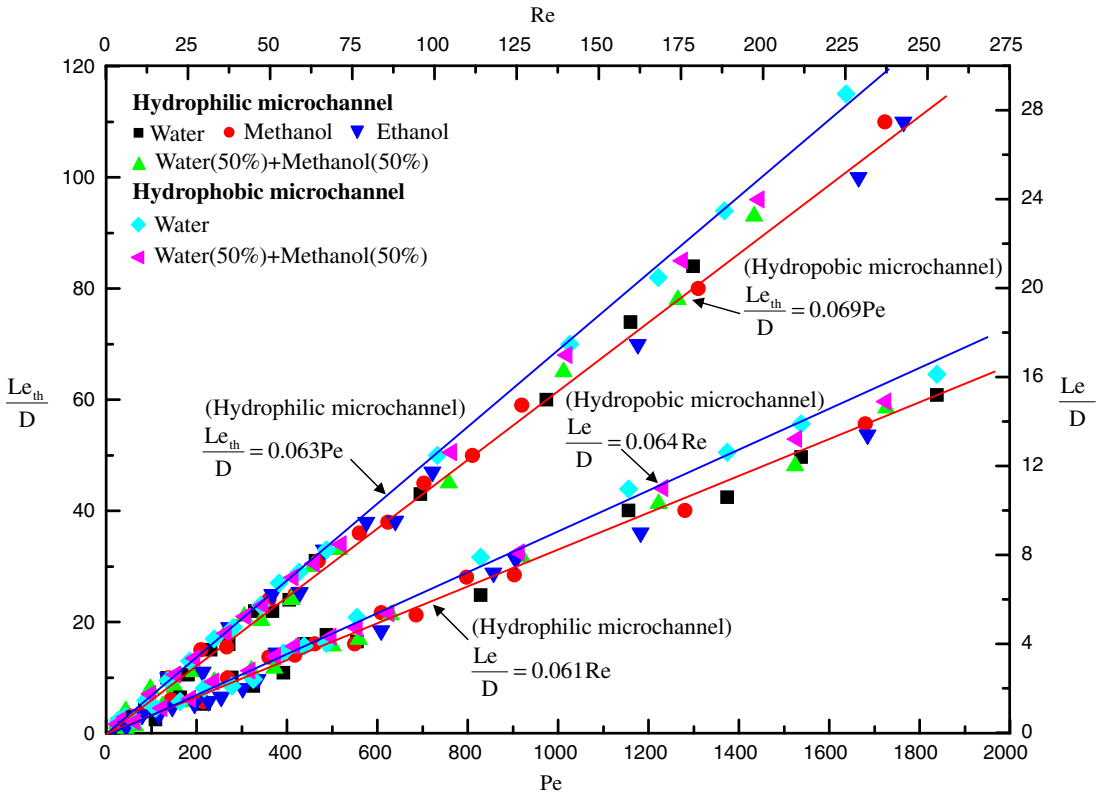

Fig. 6. The correlation of $\frac{Le_{th}}{D}$ ($\frac{Le}{D}$) vs *Pe* (*Re*) for hydrophilic and hydrophobic microchannel at constant heat flux q' = 18.1 mW/mm^2.

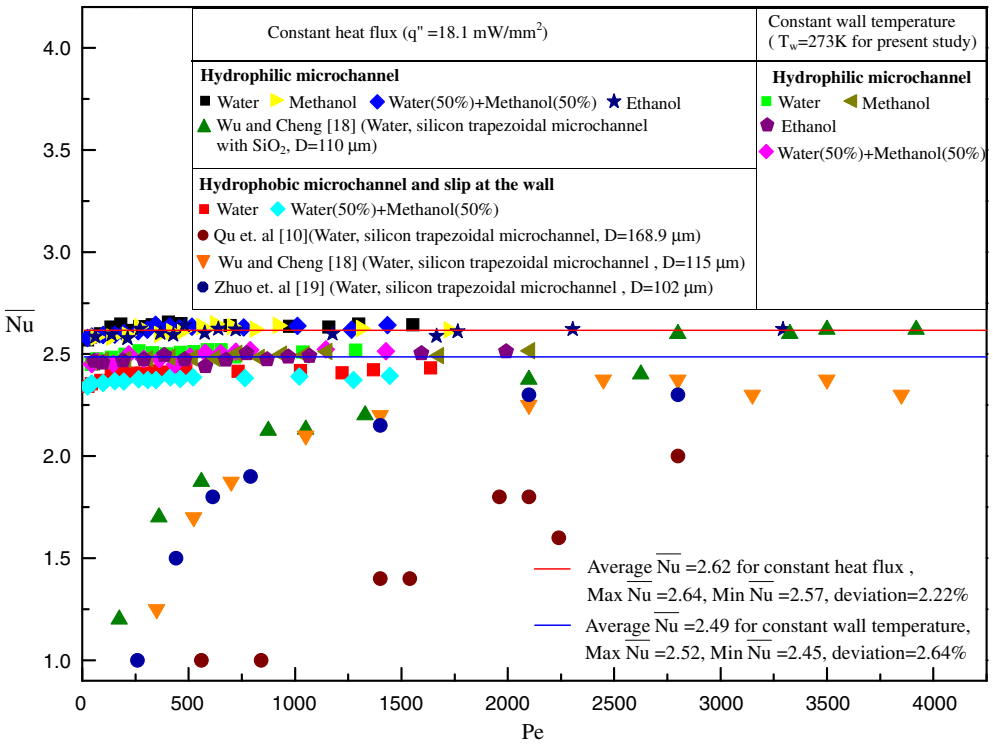

Fig. 7. The relationship of *Pe* and $\overline{Nu}$ with different working mediums in hydrophilic and hydrophobic microchannel at constant heat flux q'' = 18.1 mW/mm^2 and constant wall temperature T_w = 273 K.

$0 < Pe \leqslant 1600$; while, the heat flux has no influence on the fully developed heat transfer coefficient $\bar{h}$ and $\overline{Nu}$. Notice that the maximum surface roughness of the channel is about 3.2 nm and can be considered negligible ($\ll$D). Consequently, the surface roughness of the present microchannels appears no influence on the surface condition.

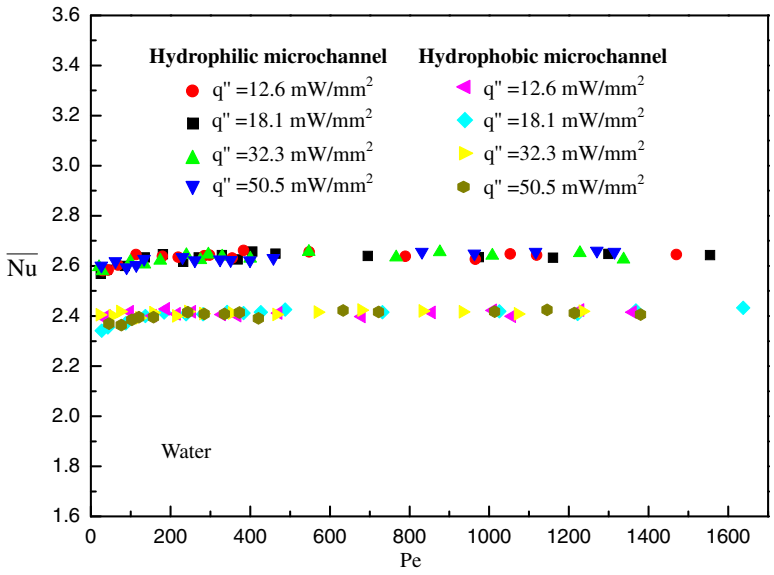

Fig. 8. $\overline{\mathrm{Nu}}$ vs *Pe* for hydrophilic and hydrophobic microchannel at four different constant heat flux (q'' = 12.6, 18.1, 32.3 and 50.5 mW/mm^2).

6. Conclusion

Liquid microchannel fluid flow and heat transfer with one-sided heating (both isothermal and isoflux) was studied for four different test fluids at $5 \leqslant Re \leqslant 240$ and the corresponding $20 \leqslant Pe \leqslant 2300$ with hydrophobic and hydrophilic surface property through μPIV for velocity and μLIF for temperature measurements. The salient feature can be drawn below:

1. Slip velocity can be found near the wall for hydrophobic microchannel from 4% to 10% associated with the working fluid of water and methanol mixture and pure water.
2. Hydrophilic microchannel consistently shows a high local/average heat transfer coefficient than that of hydrophobic microchannel for four test fluids under study although this increase is only about 8%.
3. The present constant wall temperature and constant wall heat flux fully developed heat transfer coefficient was found to be constant and independent of *Pe* regardless of what types of the test fluids are. The latter is consistently higher than that of the former as the convectional large systems do.
4. The thermal entry length was found to be a function of *Pe* and can also be correlated into a definite form of $\mathrm{Le_{th}} = 0.063(0.069)Pe$ in a hydrophilic (hydrophibic), microchannel. The coefficient of the form seems a little bit higher than the conventional one ($\sim$ 0.05 to 0.06).
5. The local Nusselt number (*Nu*) in the thermal entry region again has the following form of $Nu = 0.968\ (\mathrm{Gz}^{-1})^{-0.36}$ of $0 < \mathrm{Gz}^{-1} \leqslant 0.063$ in both hydrophilic and hydrophobic microchannels.
6. Similarly, within the thermal entry region, working fluid effect on the local heat transfer coefficient has also been found as compared to those of conventional tubes.
7. Following the above remark, surface property influence on heat transfer coefficient is further confirmed with a higher *Nu* and a little bit short hydrodyamic as well as thermal entry length for hydrophilic surface as compared to those of hydrophobic surface.
8. Heat flux has no influence on fully developed heat transfer coefficient $\overline{Nu}$ when the heat flux within the range of 12.6 mW/mm^2 $\leqslant q'' \leqslant$ 50.5 mW/mm^2.

References

[1] M. Gad-el-Hak, The MEMS Handbook, CRC Press, New York, 2002.
[2] G.E. Karniadakis, A. Beskok, Microflows: Fundamentals and Simulations, Spinger-Verlag, New York, 2002.
[3] Y. Zohar, Heat Convection in Micro Ducts, Kluwer Academic Publishers., Boston, 2003.
[4] D.B. Tuckerman, R.F. Pease, High Performance Heat Sinking for VLSI, IEEE Electronic Device Letters, EDL-2 (1981) 126–129.
[5] S.S. Hsieh, H.-H. Tsai, C.-Y. Lin, C.-F. Huang, C.-M. Chien, Gas flow in a long microchannel, International Journal of Heat and Mass Transfer 47 (2004) 3877–3887.
[6] G.P. Celata, Single-phase heat transfer and fluid flow in micropipes, Heat Transfer Engineering 25 (2004) 13–22.
[7] Gh. M. Mala, D. Li, Flow characteristics in microtubes, International Journal of Heat and Fluid Flow 20 (1999) 142–148.
[8] S.S. Hsieh, C.-Y. Lin, C.-F. Huang, H.-H. Tsai, Liquid flow in a microchannel, Intternational Journal of Micromechanics and Microengineering 14 (2004) 436–445.
[9] B.X. Wang, X.F. Peng, Experimental investigation an liquid forced convection heat transfer through microchannel, International Journal of Heat and Mass Transfer 37 (1994) 73–82.
[10] W. Qu, G.M. Mala, D. Li, Heat transfer for water flow in trapezoidal silicon microchannels, International Journal of Heat and Mass Transfer 43 (2000) 3925–3936.
[11] G.P. Celata, M. Cumo, M. Guglielmi, G. Zummo, Experimental investigation of hydraulic and single phase heat transfer in 0.130 mm capillary tube, Microscale Thermal Physical Engineering 6 (2002) 85–97.
[12] H. Herwig, O. Hausner, Critical view on new results in micro-fluid mechanics: an example, International Journal of Heat and Mass Transfer 46 (2003) 935–937.
[13] C.P. Tso, S.P. Mahulikar, Experimental verification of the role of Brinkman number in microchannels using local parameters, International Journal of Heat and Mass Transfer 43 (2000) 1837–1849.
[14] G.L. Morini, Single-phase convective heat transfer in microchannels – a review of experimental results, International Journal of Thermal Sciences 43 (2004) 631–651.
[15] F.P. Incropera, D.P. DeWitt, Fundamentals of Heat and Mass Transfer, John Wiley and Sons, New York, 1993.
[16] X.F. Peng, G.P. Peterson, B.X. Wang, Heat transfer characteristics of water flow through microchannels, Journal of Experimental Heat transfer 7 4 (1995) 264–265.
[17] X.F. Peng, G.P. Peterson, Convective heat transfer and flow friction for water flow in microchannel structures, International Journal of Heat Mass Transfer 39 (1996) 2599–2608.
[18] H.Y. Wu, P. Cheng, An experimental study of convective heat transfer in silicon microchannels with different surface conditions, International Journal of Heat and Mass Transfer 46 (2003) 2547–2556.
[19] L. Zhuo, W.Q. Tao, Y.L. He, A numerical study of laminar convective heat transfer in microchannels with non-circular cross-section, International Journal of Thermal Sciences 45 (2006) 1140–1148.

[20] P.X. Jiang, M.H. Fan, G.S. Si, Z.P. Ren, Thermal-hydraulic performance of small scale micro-channel and porous-media heat-exchanges, International Journal of Heat and Mass Transfer 44 (2001) 1039–1051.
[21] S. Shen, J.L. Xu, J.J. Zhou, Y. Chen, Flow and heat transfer in microchannels with rough wall surface, Energy Conversion and Management 47 (2006) 1311–1325.
[22] G. Hetsroni, A. Mosyak, E. Pogrebnyak, L.P. Yarin, Heat transfer in micro-channels: comparison of experiments with theory and numerical results, International Journal Heat and Mass Transfer 48 (2005) 5580–5601.
[23] Y. Mishan, A. Mosyak, E. Pogrebnyak, G. Hetsroni, Effect of developing flow and thermal regime on momentum and heat transfer in micro-scale heat sink, International Journal Heat Mass Transfer 50 (2007) 3100–3114.
[24] G.P. Celata, M. Cumo, V. Marconi, S.J. McPhail, G. Zummo, Microtube liquid single-phase heat transfer in laminar flow, International Journal of Heat and Mass Transfer 49 (2006) 3538–3546.
[25] D.C. Tretheway, C.D. Meinhart, A generating mechanism for apparent fluid slip in hydrophobic michannels, Physics of Fluids 17 (2005) 103606–103616.
[26] P. Tabeling, Introduction to Microfluidics, Oxford University Press, New York, 2005. p. 231.
[27] G.L. Morini, Analytical determination of the temperature distribution and Nusselt numbers in rectangular ducts under constant axial heat flux, International Journal of Heat and Mass Transfer 43 (2000) 741–755.